A Novel Modulated Model Predictive Control Applied to Six-Phase Induction Motor Drives

Magno Ayala, Jesus Doval-Gandoy, *Member*, *IEEE*, Jorge Rodas, *Senior Member*, *IEEE*, Osvaldo Gonzalez, Raúl Gregor *Member*, *IEEE*, and Marco Rivera *Senior Member*, *IEEE*

***Abstract*—Model-based predictive control techniques, with finite set control, are considered an interesting option to control multiphase drives due to their control flexibility and fast dynamic response. However, those techniques have some drawbacks such as a high computational cost, poor ($x - y$) currents reduction and steady-state error, especially at high speeds. To improve some of these drawbacks, modulation stages have been presented as an alternative. However, some of those drawbacks have not been improved. This paper proposes a novel approach to the classic predictive current control applied to an asymmetrical six-phase induction machine where a space vector modulation with specific vectors is used in order to improve the ($x-y$) currents, the steady-state error and total harmonic distortion at high operation speeds. Experimental results are presented to demonstrate the characteristics of the proposed control technique in terms of current tracking, ($x - y$) currents reduction and total harmonic distortion of stator currents compared to the classic predictive current control.**

***Index Terms*—Model-based predictive control, multiphase induction machine, space vector modulation.**

I. Introduction

MULTIPHASE machines have received great attention from the power electronics community due to their good features such as lower current per phase, availability, lower torque ripple and fault tolerant capabilities in comparison with traditional three-phase machines [1]. In the last few years, they were extensively applied especially in high-power applications such as electric vehicles and wind energy conversion systems [1], [2]. The majority of the control approaches applied to multiphase drives are commonly an extension of the control techniques applied to three-phase drives such as field oriented control (FOC) based on proportional-integral (PI) current control, direct torque control, among others [3], [4].

Lately, some new nonlinear control methods were developed to be applied in multiphase machines such as finite control set model predictive control (FCS-MPC), which presents fast transient response in comparison to linear controllers, addressed in [5]–[7], which has some variants already presented in the literature [8]–[10], i.e. MPC with virtual vectors (VV) which nullify the ($x - y$) currents but with a limited voltage range proposed in [11]–[13]. Another example of these variants is the modulated model predictive control (M2PC) [14], [15]. In the remainder of the paper MPC will be used instead of the cumbersome FCS-MPC as the context makes the notation clear. M2PC is designed as a conventional MPC and a modulation stage, which is based on space vector modulation (SVM). This method was presented for different power converters [16]–[18]. This technique is applied by selecting two optimal active vectors and two zero vectors, where the duty cycles are calculated through their respective cost functions. These vectors are applied by a predetermined switching pattern in order to obtain an efficient performance for the system [18]. Recently, this technique was applied to an asymmetrical six-phase induction machine (ASIMD) in [19] and it showed some improvements over classic MPC, by obtaining a fixed switching frequency and a major reduction of ($x-y$) stator currents. Still, the main drawback of classic MPC, which is the steady-state error [20], [21], was not improved with M2PC especially at high mechanical speeds.

This paper proposes a novel modulated MPC (N-M2PC) that improves the steady-state error, compared to M2PC, and reduces effectively the ($x - y$) stator currents in an ASIMD. Experimental results are presented to show the advantages of this method in terms of current tracking by considering the mean squared error (MSE), mean value and total harmonic distortion (THD) of the stator currents. This method is tested under different operation points, considering transient and steady-state conditions.

The rest of this document is organized as follows: the ASIMD mathematical model is shown in Section II. In Section III, the classic MPC design is presented as a predictive current control (PCC), where it describes the traditional PCC which will be used as a reference to the obtained results. Section IV describes the M2PC design and Section V presents the proposed N-M2PC. The experimental results show the transient and steady-state performance, for the classic PCC, PCC-VV, M2PC and N-M2PC, where the figures of merit

Manuscript received April 30, 2019; revised July 19, 2019, November 13, 2019 and January 24, 2020; accepted March 17, 2020. This work was supported by the Paraguayan Government through the CONACYT Number POSG16-05 and the Chilean Government through the FONDECYT Regular 1160690 Research Project.

M. Ayala, J. Rodas, O. Gonzalez and R. Gregor are with the Laboratory of Power and Control Systems, Facultad de Ingeniería, Universidad Nacional de Asunción, 2060 Luque, Paraguay (e-mail: mayala,jrodas,ogonzalez,rgregor@ing.una.py).

J. Doval-Gandoy is with the Applied Power Electronics Technology (APET) Research Group, University of Vigo, Vigo 36310, Spain (e-mail: jdoval@uvigo.es).

M. Rivera is with the Laboratory of Energy Conversion and Power Electronics, University of Talca, 3341717, Curicó, Chile (e-mail: marcoriv@utalca.cl).

are analyzed, in Section VI. Finally, conclusions and special remarks are presented in the last section.

II. ASIMD Mathematical Model

The selected system is composed of an ASIMD connected to a six-leg voltage source inverter (VSI) and a DC voltage source. An electrical scheme of the six-phase VSI drive, based on isolated gate bipolar transistor (IGBT), is presented in Fig. 1. The ASIMD has a continuous model which can be analyzed by differential equations. By considering the six-dimensional space of the ASIMD defined by the six-phases (a, b, c, d, e, f) and the vector space decomposition (VSD) technique, the model can be represented into three two-dimensional orthogonal planes in the stationary reference frame, $(\alpha-\beta)$, $(x-y)$ and (z_1-z_2), by using (1), where the invariant amplitude criterion has been applied [15]. The ASIMD has a phase shift of 30° between the three phases and has an isolated neutral configuration, thus (z_1-z_2) currents are assumed to be null.

$$\mathbf{T}=\frac{1}{3}\begin{array}{c}\begin{matrix}a & d & b & e & c & f\end{matrix}\\ \begin{bmatrix} 1 & \frac{\sqrt{3}}{2} & -\frac{1}{2} & -\frac{\sqrt{3}}{2} & -\frac{1}{2} & 0 \\ 0 & \frac{1}{2} & \frac{\sqrt{3}}{2} & \frac{1}{2} & -\frac{\sqrt{3}}{2} & -1 \\ 1 & -\frac{\sqrt{3}}{2} & -\frac{1}{2} & \frac{\sqrt{3}}{2} & -\frac{1}{2} & 0 \\ 0 & \frac{1}{2} & -\frac{\sqrt{3}}{2} & \frac{1}{2} & \frac{\sqrt{3}}{2} & -1 \\ 1 & 0 & 1 & 0 & 1 & 0 \\ 0 & 1 & 0 & 1 & 0 & 1 \end{bmatrix}\end{array}\begin{matrix}\alpha\\ \beta\\ x\\ y\\ z_1\\ z_2\end{matrix} \quad (1)$$

The six-phase VSI has a discrete output and a total number of $2^6=64$ switching possible states defined by the six-legs. The different switching states and the DC voltage source determine the phase voltages, which can be represented into $(\alpha-\beta)$ and $(x-y)$ planes according to the VSD approach [22]. Fig. 2 denotes the 64 possibilities which only 49 different vectors (48 vectors + 1 null vector) are considered different in the $(\alpha-\beta)$ and $(x-y)$ planes. The state-space mathematical model of the ASIMD is modeled by:

$$\dot{\mathbf{X}}_{(t)}=\mathbf{A}_{(t)}\,\mathbf{X}_{(t)}+\mathbf{B}_{(t)}\,\mathbf{U}_{(t)}+\mathbf{H}\,\varpi_{(t)} \quad (2)$$

where $\mathbf{X}_{(t)}=[x_1,\,x_2,\,x_3,\,x_4,x_5,\,x_6]^T$ is the state vector that represents the stator and rotor currents $x_1=i_{\alpha s}$, $x_2=i_{\beta s}$, $x_3=i_{xs}$, $x_4=i_{ys}$, $x_5=i_{\alpha r}$ and $x_6=i_{\beta r}$, $\mathbf{U}_{(t)}=[u_1,\,u_2,\,u_3,\,u_4]^T=[v_{\alpha s},\,v_{\beta s},\,v_{xs},\,v_{ys}]^T$ is the input vector applied to the stator coils, the process noise is represented as $\varpi_{(t)}$, $\mathbf{H}$ is considered the noise weight matrix and $\mathbf{A}_{(t)}$ and $\mathbf{B}_{(t)}$ are matrices defined by the physical parameters of the ASIMD as follows:

$$\mathbf{A}_{(t)}=\begin{bmatrix} -R_s c_2 & c_4 L_m \omega_r & 0 & 0 & c_4 R_r & c_4 L_r \omega_r \\ c_4 L_m \omega_r & -R_s c_2 & 0 & 0 & c_4 L_r \omega_r & c_4 R_r \\ 0 & 0 & -R_s c_3 & 0 & 0 & 0 \\ 0 & 0 & 0 & -R_s c_3 & 0 & 0 \\ R_s c_4 & -c_5 L_m \omega_r & 0 & 0 & -c_5 R_r & -c_5 L_r \\ -c_5 L_m \omega_r & R_s c_4 & 0 & 0 & -c_5 L_r & -c_5 R_r \end{bmatrix}$$

$$\mathbf{B}_{(t)}=\begin{bmatrix} c_2 & 0 & 0 & 0 \\ 0 & c_2 & 0 & 0 \\ 0 & 0 & c_3 & 0 \\ 0 & 0 & 0 & c_3 \\ -c_4 & 0 & 0 & 0 \\ 0 & -c_4 & 0 & 0 \end{bmatrix}$$

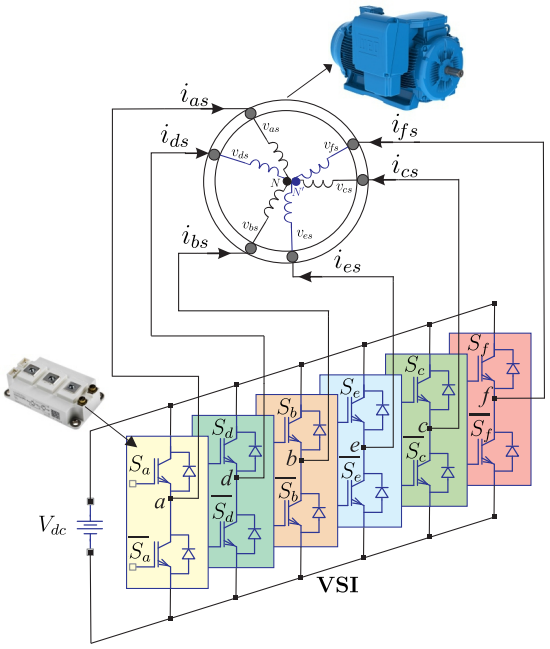

Fig. 1. Scheme of an ASIMD controlled by a six-leg VSI.

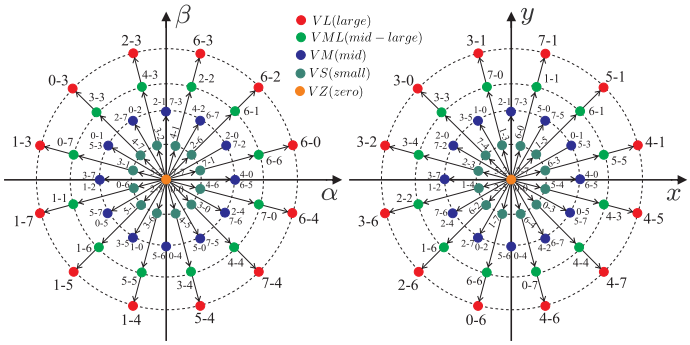

Fig. 2. Voltage space vectors and 64 switching states in $(\alpha-\beta)$ and $(x-y)$ planes for an ASIMD.

being R_s, R_r, L_m, $L_r=L_{lr}+L_m$ and $L_s=L_{ls}+L_m$ are the electrical parameters of the ASIMD. The coefficients are defined as $c_1=L_sL_r-L_m^2$, $c_2=\frac{L_r}{c_1}$, $c_3=\frac{1}{L_{ls}}$, $c_4=\frac{L_m}{c_1}$ and $c_5=\frac{L_s}{c_1}$. Stator voltages depend on the input control signals $\mathbf{S}$, which is considered the switching state. The ideal VSI model has been considered to obtain a good optimization process. Stator voltages can be estimated from the ideal six-leg VSI model $\mathbf{M}_{[\mathbf{S}]}$ [15].

$$\mathbf{M}_{[\mathbf{S}]}=\frac{1}{3}\begin{bmatrix} 2 & 0 & -1 & 0 & -1 & 0 \\ 0 & 2 & 0 & -1 & 0 & -1 \\ -1 & 0 & 2 & 0 & -1 & 0 \\ 0 & -1 & 0 & 2 & 0 & -1 \\ -1 & 0 & -1 & 0 & 2 & 0 \\ 0 & -1 & 0 & -1 & 0 & 2 \end{bmatrix}\mathbf{S}^T. \quad (3)$$

where $\mathbf{S}=[S_a,\,S_b,\,S_c,\,S_d,\,S_e,\,S_f]$, where $\mathbf{S}_i\in\{0,1\}$. The ideal six-leg VSI converts the switching gating signals into

stator voltages which are converted to $(\alpha - \beta)$ and $(x - y)$ planes and they are determined in $\mathbf{U}_{(t)}$, defined by:

$$\mathbf{U}_{(t)} = V_{dc}\, \mathbf{T}\, \mathbf{M}_{[\mathbf{S}]}. \tag{4}$$

where V_{dc} is the DC voltage source. The output vector, $\mathbf{Y}$, is:

$$\mathbf{Y}_{(t)} = \mathbf{C}\, \mathbf{X}_{(t)} + \nu_{(t)} \tag{5}$$

where $\nu_{(t)}$ is considered the measurement noise and

$$\mathbf{C} = \begin{bmatrix} 1 & 0 & 0 & 0 & 0 & 0 \\ 0 & 1 & 0 & 0 & 0 & 0 \\ 0 & 0 & 1 & 0 & 0 & 0 \\ 0 & 0 & 0 & 1 & 0 & 0 \end{bmatrix}.$$

The mechanical variables of the ASIMD are related by:

$$T_e = 3\, P\, (\psi_{\alpha s} i_{\beta s} - \psi_{\beta s} i_{\alpha s}) \tag{6}$$

$$J_i\, \dot{\omega}_m + B_i\, \omega_m = (T_e - T_L) \tag{7}$$

$$\omega_r = P \omega_m \tag{8}$$

where J_i is the inertia coefficient, B_i is considered the friction coefficient, T_e represents the electromagnetic torque, T_L is the load torque, ω_r is the rotor electrical angular speed, ω_m the rotor mechanical speed, $\psi_{\alpha s}$ and $\psi_{\beta s}$ are considered the stator fluxes and P the number of pole pairs.

III. Classic PCC

The mathematical model of the ASIMD (2) and (5) must be in discrete form so it can be applied for the PCC. A forward-Euler method is considered to maintain a low computational cost for the controller. The equations will be in digital form with predicted variables only depending on past values of the variables and not on present values. Thus, a prediction of the next sample state $\hat{\mathbf{X}}_{[k+1|k]}$ is defined as:

$$\hat{\mathbf{X}}_{[k+1|k]} = \mathbf{X}_{[k]} + \mathrm{f}\left(\mathbf{X}_{[k]},\, \mathbf{U}_{[k]},\, T_s,\, \omega_{r[k]}\right) \tag{9}$$

being $[k]$ the current sample, f the function nomenclature and T_s is the sampling time.

A. Reduced Order Observers

In the state-space modeling (2), only the stator currents and mechanical rotor speed are measured. The stator voltages are easily estimated from the switching commands sent to the six-phase VSI. However, the rotor currents are rarely measured in real system and they have to be estimated. This issue can be solved by the estimation of the rotor currents through the concept of reduced order observers. The reduced order observers only estimate the value of the unmeasured parts of the state vector. This is an important topic which has been recently solved by the use of Luenberger Observer (LO) [23] and Kalman Filter (KF) [9], [24] techniques, where the KF is considered a better selection due to the fact that the observer gains are optimized taking into account the noise input to the sensors. In LO-based estimator, the gains are not so optimized and the setting is deterministic [9]. Therefore, KF is designed and implemented in this paper to improve the control performance of PCC, by increasing the accuracy of the predictions. By considering zero-mean Gaussian measurement noises and uncorrelated process, the equations of the system state-space mathematical model can be defined as:

$$\hat{\mathbf{X}}_{[k+1|k]} = \mathbf{A}_{[k]}\mathbf{X}_{[k]} + \mathbf{B}_{[k]}\mathbf{U}_{[k]} + \mathbf{H}\varpi_{[k]} \tag{10}$$

$$\mathbf{Y}_{[k+1|k]} = \mathbf{C}\, \mathbf{X}_{[k+1]} + \nu_{[k+1]} \tag{11}$$

where $\mathbf{A}_{[k]}$ and $\mathbf{B}_{[k]}$ are defined by (12)-(14). It can be noted that $\mathbf{A}_{[k]}$ is also dependable on the present value of $\omega_{r[k]}$ and consequently must be considered at every sampling period. A detailed explanation of the dynamics and error convergence of the KF can be found in [9], [24] and it was not included in this work for the sake of conciseness. The aforementioned matrices are defined as:

$$\mathbf{A}_{[k]} = \begin{bmatrix} A_{11} & A_{12} & 0 & 0 & A_{15} & A_{16} \\ A_{21} & A_{22} & 0 & 0 & A_{25} & A_{26} \\ 0 & 0 & A_{33} & 0 & 0 & 0 \\ 0 & 0 & 0 & A_{44} & 0 & 0 \\ A_{51} & A_{52} & 0 & 0 & A_{55} & A_{56} \\ A_{61} & A_{62} & 0 & 0 & A_{65} & A_{66} \end{bmatrix} \tag{12}$$

where $\mathbf{A}_{[k]}$ parameters are defined as follows:

$$\begin{aligned} A_{11} &= A_{22} = 1 - T_s c_2 R_s \\ A_{12} &= -A_{21} = T_s c_4 L_m \omega_{r[k]} \\ A_{15} &= A_{26} = T_s c_4 R_r \\ A_{16} &= -A_{25} = T_s c_4 L_r \omega_{r[k]} \\ A_{33} &= A_{44} = 1 - T_s c_3 R_s \\ A_{51} &= A_{62} = -T_s c_4 R_s \\ A_{52} &= -A_{61} = -T_s c_5 L_m \omega_{r[k]} \\ A_{55} &= A_{66} = 1 - T_s c_5 R_r \\ A_{56} &= -A_{65} = -c_5 \omega_{r[k]} T_s L_r \end{aligned} \tag{13}$$

$$\mathbf{B}_{[k]} = \begin{bmatrix} B_{11} & 0 & 0 & 0 & 0 & 0 \\ 0 & B_{22} & 0 & 0 & 0 & 0 \\ 0 & 0 & B_{33} & 0 & 0 & 0 \\ 0 & 0 & 0 & B_{44} & 0 & 0 \\ 0 & 0 & 0 & 0 & B_{55} & 0 \\ 0 & 0 & 0 & 0 & 0 & B_{66} \end{bmatrix} \tag{14}$$

being $\mathbf{B}_{[k]}$ parameters the following: $B_{11} = B_{22} = T_s c_2$, $B_{33} = B_{44} = T_s c_3$ and $B_{55} = B_{66} = -T_s c_4$

B. Cost Function

The cost function problem can allow the optimization of several important variables such as machine torque ripple minimization, VSI switching losses and harmonic content minimization [20]. However in current control, the most important figure of merit is the tracking error in the predicted stator currents in $(\alpha - \beta)$ and $(x - y)$ planes. PCC analyses the cost function for 49 iterations with the following:

$$J_{[k+2|k]} = \Bigg[(i^*_{\alpha s[k+2]} - \hat{i}_{\alpha s[k+2|k]})^2 + (i^*_{\beta s[k+2]} - \hat{i}_{\beta s[k+2|k]})^2 + \lambda_{xy} \left((i^*_{xs[k+2]} - \hat{i}_{xs[k+2|k]})^2 + (i^*_{ys[k+2]} - \hat{i}_{ys[k+2|k]})^2 \right) \Bigg]^{\frac{1}{2}} \tag{15}$$

By using (16), a second-step ahead prediction of the stator currents $\hat{i}_{s[k+2|k]}$ is computed for delay compensation [25]. The desired reference trajectory of the stator currents is represented by $i^*_{s[k+2]}$. The weighting factor optimization is a hot research topic and some recent works tackled this issue [7], [26], [27]. Typically, for multiphase machines, λ_{xy} allows to prioritize the stator currents in $(\alpha - \beta)$ plane [9], [28].

$$\hat{\mathbf{X}}_{[k+2|k]} = \mathbf{A}_{[k]}\mathbf{X}_{[k+1]} + \mathbf{B}_{[k]}\mathbf{U}_{[k+1]} + \mathbf{H}\varpi_{[k]} \tag{16}$$

IV. M2PC

This technique consists in the determination of each available sector for the six-leg VSI in the $(\alpha - \beta)$ plane, being 48 sectors in total, which are composed of two adjacent active vectors and a null vector (VZ), as shown in Fig. 3. This technique, which is based on SVM, estimates the prediction of two active vectors that conform the 12 outside sectors at every sampling time and analyses their respective cost functions (J_0, J_1 and J_2) separately. Each prediction is evaluated based on (15) and the only difference is in the calculation of the input voltage vector $\mathbf{U}_{[k]}$ [15], [19]. The main goal of this modulation technique is to obtain any voltage vector in the $(\alpha - \beta)$ plane by using the large vectors (VL) and the VZ, covering the entire space vector, and at the same time, note that the outside vectors are the smallest voltage vectors in $(x - y)$ plane, managing a reduction of $(x - y)$ currents [19].

The duty cycles, for the two active vectors d_1 and d_2, are obtained by solving the following equations, related to their respective cost functions (24 for every sample time):

$$d_0 = \frac{\sigma}{J_0} \qquad d_1 = \frac{\sigma}{J_1} \qquad d_2 = \frac{\sigma}{J_2} \tag{17}$$

$$d_0 + d_1 + d_2 = 1 \tag{18}$$

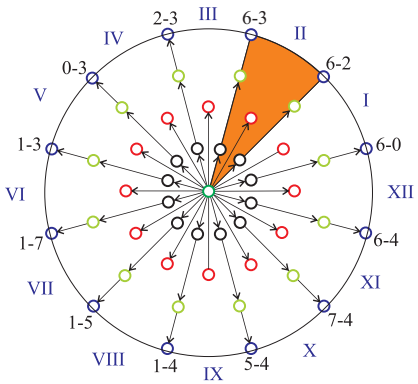

Fig. 3. Available sectors for the six-leg VSI.

where d_0 is the duty cycle of a null vector. Then, it is possible to calculate the expression for σ and the duty cycles for each vector given as:

$$J_T = J_1J_2 + J_0J_1 + J_0J_2 \tag{19}$$

$$d_0 = \frac{J_1J_2}{J_T} \tag{20}$$

$$d_1 = \frac{J_0J_2}{J_T} \tag{21}$$

$$d_2 = \frac{J_0J_1}{J_T} \tag{22}$$

Considering these expressions, the final cost function, which is calculated for 12 iterations during T_s, is considered as:

$$G_{[k+2|k]} = d_1J_1 + d_2J_2 \tag{23}$$

The two vectors, which reduce $G_{[k+2|k]}$, are selected and applied to the six-phase VSI at the next sampling time. After calculating the duty cycles for the two vectors to be applied, it is necessary to propose an equation relating the duty cycles and the selected voltage vectors, in order to implement a symmetric pulse width modulation (PWM):

$$\tau_i = \frac{d_0}{2} + d_1v_{1(i)} + d_2v_{2(i)} \tag{24}$$

where $i = [a, b, c, d, e, f]$ and τ_i is the duty cycle per phase. This variable is compared to a triangular waveform to obtain the respective symmetric PWM, accomplishing a fixed switching frequency fixing the sampling frequency.

V. N-M2PC

As well as M2PC, N-M2PC is also based on SVM. The main difference is that M2PC only uses 2 VL per sector and N-M2PC uses 4 which include 2 mid vectors (VM) and 2 VL. The main goal of this modulation is to improve further the steady-state error of the stator currents tracking in $(d - q)$ plane by including these adjacent VM per sector in order to avoid the application of VZ which limits the range. This is due to the fact that the desired optimal vector is within the corresponding sector and a certain combination of vector can represent that particular optimal vector. However, VZ reduces the range of the combination of vectors with its corresponding duty cycle, reducing the controller's capacity of tracking the desired stator current in $(\alpha - \beta)$ plane, due to the fact that the duty cycle of VZ increases when the $(x - y)$ currents are being reduced in M2PC. In summary, N-M2PC does not have the same limitation as M2PC, due to the fact that it does not apply VZ and the used vectors add any point in the upper area of the $(\alpha - \beta)$ plane.

The duty cycles, for the four active vectors d_1, d_2, d_3 and d_4, are obtained by solving the following equations:

$$d_1 = \frac{\sigma}{J_1} \quad d_2 = \frac{\sigma}{J_2} \quad d_3 = \frac{\sigma}{J_3} \quad d_4 = \frac{\sigma}{J_4} \tag{25}$$

$$d_1 + d_2 + d_3 + d_4 = 1 \tag{26}$$

where J_1, J_2, J_3 and J_4 are the corresponding cost function (15) for the vectors in the selected sector. As M2PC, it is

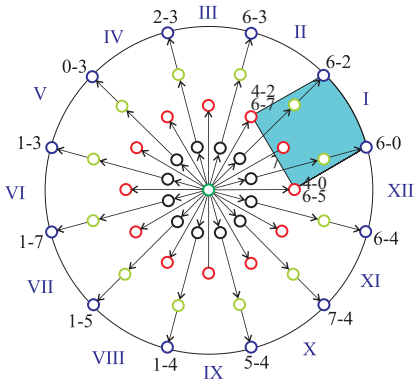

Fig. 4. Available sectors of N-M2PC for the six-leg VSI.

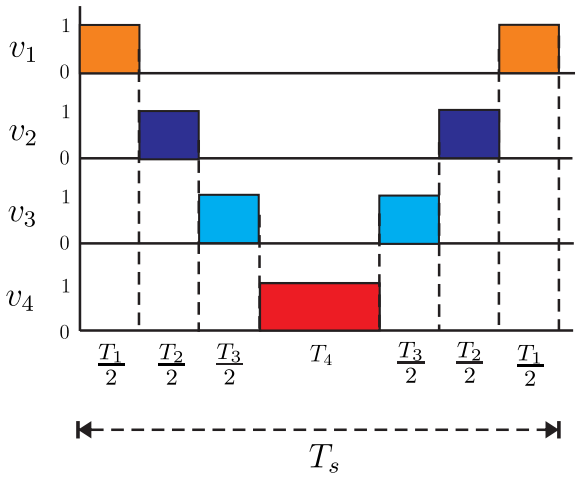

Fig. 5. Switching pattern for the selected optimal vectors.

possible to calculate the expression for σ and the duty cycles for each vector given as:

$$J_{T1} = J_1 J_3 J_4 + J_2 J_3 J_4 \tag{27}$$

$$J_{T2} = J_1 J_2 J_4 + J_1 J_2 J_3 \tag{28}$$

$$d_1 = \frac{J_2 J_3 J_4}{J_{T1} + J_{T2}} \tag{29}$$

$$d_2 = \frac{J_1 J_3 J_4}{J_{T1} + J_{T2}} \tag{30}$$

$$d_3 = \frac{J_1 J_2 J_4}{J_{T1} + J_{T2}} \tag{31}$$

$$d_4 = \frac{J_1 J_2 J_3}{J_{T1} + J_{T2}} \tag{32}$$

N-M2PC evaluates all the 12 sectors, as shown in Fig. 4, by calculating the corresponding cost function for each vector (48 in total), then the duty cycles of each vector is calculated as in M2PC, at last, the final cost function is computed as:

$$G_{[k+2|k]} = d_1 J_1 + d_2 J_2 + d_3 J_3 + d_4 J_4 \tag{33}$$

It can be noticed that the VM used to obtain the 12 sectors are the redundant ones, giving the possibility to select each of those vectors in order to apply a certain switching pattern, as the one shown in Fig. 5. This allows the use of a simple equation to calculate the duty cycles $\tau_{(i)}$ for the switching devices of each leg of the VSI, as follows:

$$\tau_{(i)} = d_1 v_{1(i)} + d_2 v_{2(i)} + d_3 v_{3(i)} + d_4 v_{4(i)} \tag{34}$$

where $\tau_{(i)}$ is normalized between 0 and 1, for the switching devices for the six-phase legs VSI. At last, a triangular carrier waveform is used to apply the value of $\tau_{(i)}$ in the corresponding switching devices.

VI. Experimental Results

The proposed N-M2PC technique is validated in order to compare its performance with M2PC and classic PCC through experimental results obtained in the test bench.

A. Test bench composition

The test bench is composed of an ASIMD connected to two conventional three-phase VSI, using a constant DC-bus voltage from a DC power supply. The six-phase VSI is controlled by a dSPACE MABXII DS1401 real-time rapid prototyping platform, with MATLAB/Simulink. The results are processed using MATLAB R2013b script. Table I shows the electrical and mechanical parameters of the ASIMD obtained using stand-still with VSI tests and conventional methods of AC time domain [29], [30]. The experimental measurements were obtained with current sensors LA 55-P s, with several turns to improve precision at low current measurement, which have a frequency bandwidth from DC up to 200 kHz. Those values are then converted to digital through 16-bit A/D converter. The ASIMD rotor angle is measured with a 1024 ppr incremental encoder and the mechanical speed is calculated from it. Finally, a 5 HP eddy current brake is used as a variable mechanical load on the ASIMD which is fixed at 1 A. A block diagram of the test bench is shown in Fig. 6. The defined cost function in (15) with λ_{xy} = 0.05 was selected to evaluate the performance of classic PCC, which its influence in the performance is minimal, and M2PC giving more priority to $(\alpha - \beta)$ stator currents tracking over the $(x - y)$ currents reduction. As for N-M2PC, λ_{xy} = 0.1 is selected, due to the fact that it does not use the null vector and the $(x - y)$ currents reduction is obtained through the active vectors combination. It is worth

TABLE I
PARAMETERS OF THE ASIMD.

PARAMETER	VALUE	PARAMETER	VALUE
R_r (Ω)	6.9	R_s (Ω)	6.7
L_s (mH)	654.4	L_r (mH)	626.8
L_m (mH)	614	L_{ls} (mH)	5.3
ω_{m-nom} (rpm)	3 000	P_w (kW)	2
J_i (kg.m^2)	0.07	B_i (kg.m^2/s)	0.0004
P	1	V_{dc} (V)	400

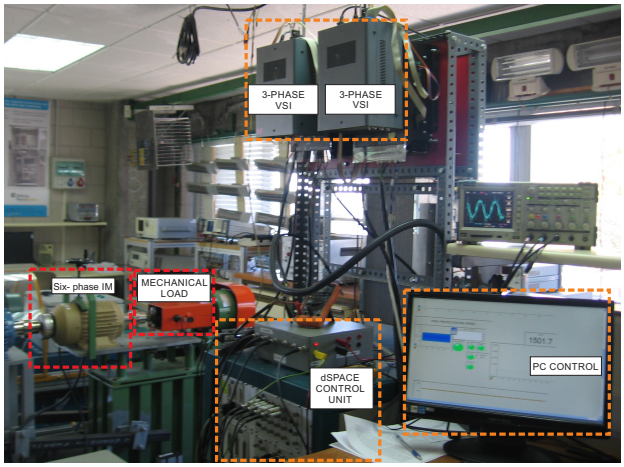

Fig. 6. Block diagram of the test bench including the ASIMD, the dSPACE platform, the eddy current brake and the six-phase VSI.

mentioning that these values of λ_{xy} are selected through heuristic method by focusing on obtaining a sub-optimal system. The process and measurement noise values can be calculated by using the autocovariance-least-squared (ALS) method since provides unbiased estimates with the lowest covariance, guaranteeing optimal KF tuning. By collecting data from a closed-loop operation of the system and then using the method proposed in [24]. The obtained values are $\hat{Q}_w = 0.0022$ and $\hat{R}_v = 0.0022$.

B. Figures of merit

The performance of the proposed N-M2PC is analyzed and compared to classic PCC and M2PC in transient and steady-state conditions. The experimental results analyze the controller performance in terms of MSE between the reference and measured stator currents in $(\alpha - \beta)$ and $(x - y)$ planes. At the same time, the mean value error of $(d-q)$ currents are analyzed to obtain the steady-state error in current tracking for the three techniques. At last, THD is calculated in $(\alpha - \beta)$ plane to complete the analysis. The MSE is defined as:

$$\text{MSE}(i_{s\Phi}) = \sqrt{\frac{1}{N}\sum_{k=1}^{N}(i_{s\Phi}[k] - i^*_{s\Phi}[k])^2} \tag{35}$$

where N is the number of analyzed samples, $i^*_{s\Phi}$ the stator current reference, $i_{s\Phi}$ the measured stator currents and $\Phi \in \{\alpha,\ \beta,\ x,\ y\}$. On the other hand, the mean value is calculated as:

$$\text{Error}(\%)(i_{s\theta}) = |\frac{100}{N}\sum_{k=1}^{N} i_{s\theta}[k] - i^*_{s\theta}[k]| \tag{36}$$

where $i^*_{s\theta}$ is $(d - q)$ stator currents reference and $i_{s\theta}$ the measured $(d - q)$ stator currents. At last, THD is defined as:

$$\text{THD}(i_s) = \sqrt{\frac{1}{i_{s1}^2}\sum_{j=2}^{N}(i_{sj})^2} \tag{37}$$

TABLE II
PERFORMANCE ANALYSIS OF STATOR CURRENTS, MSE (A), MEAN ERROR (%) FOR CLASSIC PCC AT DIFFERENT ROTOR SPEEDS (RPM).

		Sampling	frequency	8 kHz		
ω_m^*	MSE_α	MSE_β	MSE_x	MSE_y	Error_d	Error_q
500	0.1437	0.1282	0.8228	0.8158	1.48	9.41
1000	0.1443	0.1372	0.9605	0.9570	0.54	7.02
1500	Uns	Uns	Uns	Uns	Uns	Uns
2000	Uns	Uns	Uns	Uns	Uns	Uns
		Sampling	frequency	16 kHz		
ω_m^*	MSE_α	MSE_β	MSE_x	MSE_y	Error_d	Error_q
500	0.0831	0.0755	0.4676	0.4763	0.70	3.70
1000	0.0974	0.0858	0.5087	0.5072	0.24	3.79
1500	0.0812	0.0771	0.5185	0.5057	1.48	3.45
2000	Uns	Uns	Uns	Uns	Uns	Uns

TABLE III
PERFORMANCE ANALYSIS OF STATOR CURRENTS, MSE (A), MEAN ERROR (%) FOR PCC-VV AT DIFFERENT ROTOR SPEEDS (RPM).

		Sampling	frequency	8 kHz		
ω_m^*	MSE_α	MSE_β	MSE_x	MSE_y	Error_d	Error_q
500	0.1623	0.1620	0.0856	0.0784	0.94	6.23
1000	0.1682	0.1691	0.0905	0.0904	1.02	6.52
1500	Uns	Uns	Uns	Uns	Uns	Uns
2000	Uns	Uns	Uns	Uns	Uns	Uns
		Sampling	frequency	16 kHz		
ω_m^*	MSE_α	MSE_β	MSE_x	MSE_y	Error_d	Error_q
500	0.1256	0.1182	0.0640	0.0600	0.86	4.11
1000	0.1299	0.1231	0.0810	0.0638	0.89	4.46
1500	0.1445	0.1231	0.0760	0.0714	6.26	5.89
2000	0.1455	0.1309	0.0860	0.0838	6.50	8.95

where i_{s1} is the fundamental stator currents and i_{sj} is the harmonic stator currents.

C. Steady state analysis

For all cases, $(x - y)$ current references are set to zero ($i^*_{xs} = i^*_{ys} = 0$). A fixed d current ($i^*_{ds} = 1$ A) has been used. The sampling frequencies used in the tests are 8 kHz and 16 kHz. Four steady-state operations are set for mechanical speed: 500 rpm, 1 000 rpm, 1 500 rpm and 2 000 rpm.

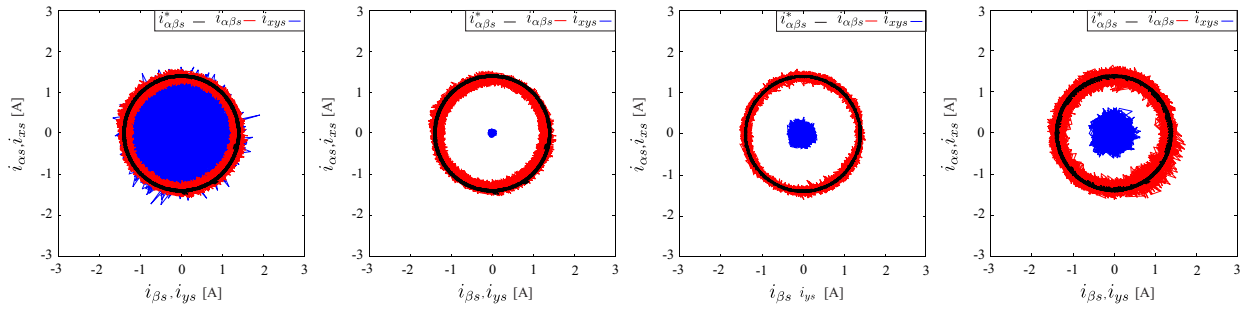

Fig. 7. Stator currents in $(\alpha-\beta)$ and $(x-y)$ planes at 500 rpm for: (a)classic PCC; (b)PCC-VV; (c)M2PC; (d)N-M2PC.

TABLE V
PERFORMANCE ANALYSIS OF STATOR CURRENTS, MSE (A), MEAN ERROR (%) FOR N-M2PC AT DIFFERENT ROTOR SPEEDS (RPM).

		Sampling	frequency	8 kHz		
ω_m^*	MSE_α	MSE_β	MSE_x	MSE_y	Error_d	Error_q
500	0.1977	0.1998	0.2490	0.2553	1.8	2.6
1000	0.2135	0.2159	0.2659	0.2684	3.3	6.9
1500	0.1983	0.1924	0.3012	0.2956	2.25	13.8
2000	0.2033	0.2062	0.3020	0.3020	5.32	18.2
		Sampling	frequency	16 kHz		
ω_m^*	MSE_α	MSE_β	MSE_x	MSE_y	Error_d	Error_q
500	0.1004	0.1003	0.2009	0.2130	0.81	2.52
1000	0.1051	0.1049	0.2091	0.2064	1.04	4.84
1500	0.1030	0.1097	0.2172	0.2125	1.97	5.72
2000	0.1084	0.1081	0.2325	0.2287	1.99	8.71

TABLE IV
PERFORMANCE ANALYSIS OF STATOR CURRENTS, MSE (A), MEAN ERROR (%) FOR M2PC AT DIFFERENT ROTOR SPEEDS (RPM).

		Sampling	frequency	8 kHz		
ω_m^*	MSE_α	MSE_β	MSE_x	MSE_y	Error_d	Error_q
500	0.0562	0.0592	0.1241	0.1130	1.34	2.69
1000	0.0861	0.0903	0.1485	0.1545	1.9	7.03
1500	0.1039	0.0958	0.1960	0.1944	2.2	7.33
2000	Uns	Uns	Uns	Uns	Uns	Uns
		Sampling	frequency	16 kHz		
ω_m^*	MSE_α	MSE_β	MSE_x	MSE_y	Error_d	Error_q
500	0.1046	0.1094	0.1332	0.1334	0.51	3.04
1000	0.1037	0.1059	0.1401	0.1417	0.14	4.59
1500	0.0972	0.0986	0.1038	0.1069	0.4	5.93
2000	0.0976	0.0989	0.1150	0.1182	0.26	9.04

Table II shows the experimental results obtained for different mechanical speeds and sampling frequencies for classic PCC, regarding the MSE of stator currents in $(\alpha-\beta)$ and $(x-y)$ planes and Mean Error (%) in $(d-q)$ planes. The results show good performance of classic PCC in terms of $(\alpha-\beta)$ current tracking and steady-state error for $(d-q)$ currents at a higher sampling frequency compared to lower sampling frequency. However, the $(x-y)$ reduction is insufficient, and the performance is worse at higher mechanical speed to the point of becoming unstable (Uns) at low sampling frequency, where the error system is tending towards infinity due to the fact that parameters such as sampling time, rotor speed, electrical parameters have a direct impact on the poles placement of the ASIMD [31].

TABLE VI
PERFORMANCE ANALYSIS OF STATOR CURRENTS, THD (%) FOR CLASSIC PCC, PCC-VV, M2PC AND N-M2PC AT DIFFERENT SPEEDS (RPM).

Sampling frequency of 8 kHz				
	PCC	PCC-VV	M2PC	N-M2PC
ω_m^*	$\text{THD}_{\alpha\beta}$	$\text{THD}_{\alpha\beta}$	$\text{THD}_{\alpha\beta}$	$\text{THD}_{\alpha\beta}$
500	12.84	13.78	5.39	15.78
1000	14.27	14.85	7.38	14.42
1500	Uns	Uns	8.16	17.98
2000	Uns	Uns	Uns	17.65
Sampling frequency of 16 kHz				
	PCC	PCC-VV	M2PC	N-M2PC
ω_m^*	$\text{THD}_{\alpha\beta}$	$\text{THD}_{\alpha\beta}$	$\text{THD}_{\alpha\beta}$	$\text{THD}_{\alpha\beta}$
500	7.55	12.57	10.61	9.95
1000	8.41	12.49	10.17	9.73
1500	7.27	12.70	8.10	9.78
2000	Uns	13.23	7.65	9.54

Table III presents the performance of PCC-VV which improves the reduction of $(x-y)$ currents compared to classic PCC. On the other hand, Table IV shows the results of M2PC which show a far better performance at lower sampling frequency and lower mechanical speed in all the figures of merit, compared to classic PCC. However, the performance also worsens at higher sampling frequency and mechanical speed, specially in steady-state error for $(d-q)$ currents. Table V exposes the N-M2PC performance in terms of the current tracking and steady-state error in $(d-q)$ currents. It can be seen that N-M2PC improves the steady-state error in $(d-q)$ currents and $(x-y)$ currents reduction compared to classic PCC, but M2PC is better in every aspect, except at high mechanical speeds where N-M2PC is the only stable controller. At higher sampling frequency, N-M2PC is better in every figure of merit in comparison lower sampling frequency and is comparable to M2PC in every figure of merit.

Table VI shows the THD in $(\alpha-\beta)$ stator currents for Classic PCC, M2PC and N-M2PC for different mechanical speeds. The results present a reduction on the THD

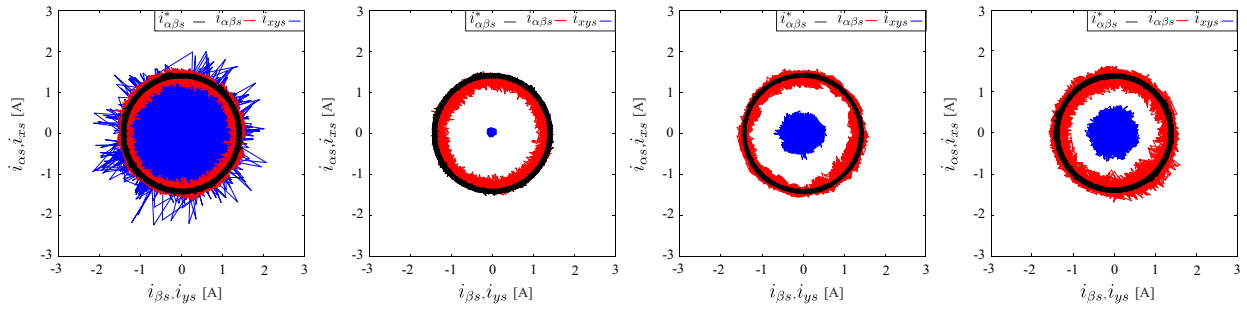

Fig. 8. Stator currents in $(\alpha - \beta)$ and $(x - y)$ planes at 1500 rpm for: (a)classic PCC; (b)PCC-VV; (c)M2PC; (d)N-M2PC.

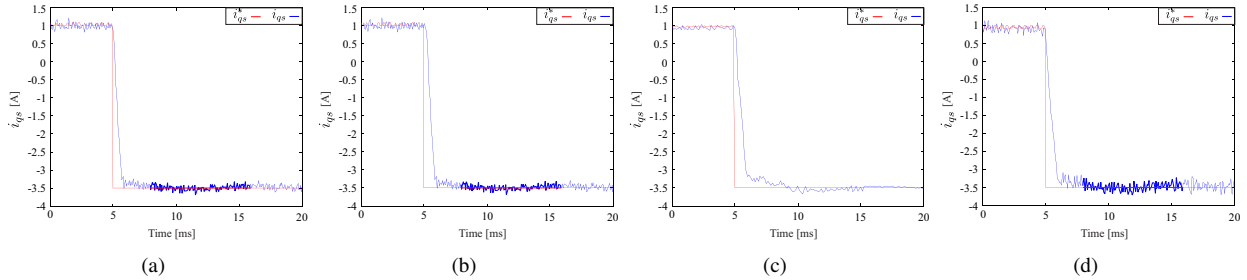

Fig. 9. Transient response of stator current (q) from a step response of 1 A to -3.5 A for different techniques: (a)classic PCC; (b)PCC-VV; (c)M2PC; (d)N-M2PC.

TABLE VII
IMPROVEMENT ANALYSIS (%) OF M2PC AND N-M2PC OVER CLASSIC PCC AT DIFFERENT SPEEDS (RPM).

ω^*_m	MSE$_{\alpha\beta}$	MSE$_{xy}$	Error$_d$	Error$_q$	THD$_{\alpha\beta}$
	Sampling	frequency	8 kHz	(M2PC)	
500	57.36	85.53	9.46	71.41	57.73
1000	37.26	84.20	-251.85	-0.14	46.86
1500	100	100	100	100	100
2000	–	–	–	–	–
	Sampling	frequency	8 kHz	(N-M2PC)	
500	-46.71	69.22	-21.62	72.37	-23.38
1000	-52.66	72.14	-511.11	1.71	-1.12
1500	100	100	100	100	100
2000	100	100	100	100	100
	Sampling	frequency	16 kHz	(M2PC)	
500	-35.39	71.75	27.14	17.84	-41.25
1000	-14.95	72.94	41.67	-21.11	-21.76
1500	-23.80	79.42	72.97	-71.88	-11.74
2000	100	100	100	100	100
	Sampling	frequency	16 kHz	(N-M2PC)	
500	-26.83	56.16	-15.71	31.89	-32.59
1000	-15.08	59.10	-333.33	-27.70	-16.50
1500	-34.57	58.04	-33.11	-65.80	-35.21
2000	100	100	100	100	100

stator currents with higher sampling frequency and higher mechanical speed for classic PCC. For M2PC, the currents THD are better at lower mechanical speed at low sampling frequency, M2PC changes its tendency at high sampling frequency. As for N-M2PC, the THD improves at high sampling frequency and is consistent for every operation.

Fig. 7 and Fig. 8 present the stator currents performance with a polar representation in $(\alpha - \beta)$ and $(x - y)$ planes for classic PCC, PCC-VV, M2PC and N-M2PC. The operations were tested with different eddy current (mechanical load), thus the value of $(\alpha - \beta)$ amplitude is the same at different mechanical speeds. The figures show that $(x - y)$ currents are lower for N-M2PC and especially for M2PC and PCC-VV compared to classic PCC. At last, Table VII presents the performance of M2PC and N-M2PC compared to classic PCC in terms of %, where positive $(+)$ and negative $(-)$ values mean improvement and deterioration respectively.

D. Transient analysis

For a transient condition, a step modification in mechanical speed is considered from 500 to -500 rpm (reversal operation). Fig. 9 exposes a dynamic test (performance of q axis current), which consists of the transient behavior of classic PCC, PCC-VV, M2PC and N-M2PC for a step response in the q axis current (i^*_{qs}). The dynamic response is generated through a reversal operation of the mechanical speed (ω_m) from 500 to -500 rpm. Fig. 9(a) and Fig. 9(b) show a transient test for classic PCC and PCC-VV where the time to reach the new reference is approximately 1 ms. Fig. 9(c) and Fig. 9(d) show the dynamic response of M2PC and N-M2PC, which they present a reaching time of 4 and 3 ms respectively.

E. Robustness analysis

The robustness analysis consists in the performance comparison of the controller at a nominal L_m value and with a variation of 25% of its nominal value, being L_m

TABLE VIII
PERFORMANCE ANALYSIS OF STATOR CURRENTS FOR N-M2PC UNDER 25% OF VARIATION OF THE NOMINAL L_m.

		Sampling	frequency	8 kHz		
ω_m^*	MSE_α	MSE_β	MSE_x	MSE_y	$Error_d$	$Error_q$
500	0.2175	0.2270	0.2706	0.2721	1.48	11.07
1000	0.2332	0.2389	0.3061	0.3009	6.43	13.82
1500	0.2006	0.2027	0.3019	0.3000	1.87	16.2
2000	0.2094	0.2065	0.3120	0.3096	4.70	19.66
		Sampling	frequency	16 kHz		
ω_m^*	MSE_α	MSE_β	MSE_x	MSE_y	$Error_d$	$Error_q$
500	0.1145	0.1057	0.2056	0.2130	0.21	3.23
1000	0.1168	0.1157	0.2027	0.2014	0.21	5.30
1500	0.1199	0.1195	0.2042	0.2118	0.95	6.77
2000	0.1219	0.1181	0.2125	0.2200	2.26	8.09

TABLE IX
COMPARATIVE ANALYSIS OF COMPUTATIONAL COST OF CLASSIC PCC, PCC-VV, M2PC AND N-M2PC IN TERMS OF FPOS.

	PCC	PCC-VV	M2PC	N-M2PC
FPOs	2352	1452	1968	2736

the most sensitive parameter in induction machines [32], [33]. This is analyzed by taking in consideration the effect of magnetic saturation of the ASIMD, where L_m value typically changes in approximately that ratio. Table VIII presents the control performance with a L_m change of 25% of the nominal value to analyze the control robustness to uncertainties. The results show that at low speed, the control performance presents a good tracking of stator currents with a variation of approximately 12% and 11%, compared to the unmodified L_m value, for 500 and 1000 rpm respectively, showing an low sensibility in these operation points. On the other hand, at higher speed, the control performance also shows a good current tracking with a variation of approximately 14% and 8%, showing a good robustness at 1500 and 2000 rpm. However, the steady state error in $(d-q)$ currents is severely affected in all the mechanical speeds at 8 kHz, being approximately 5 and 2 times higher, but minimal change in steady state error is obtained, at 16 kHz, of approximately 16%, presenting a good performance at that sampling frequency.

F. Comparative analysis

A comparative analysis regarding computational cost for classic PCC, M2PC and N-M2PC. It is considered the number of floating point operations (FPOs) per technique and then summarized on Table IX. For classic PCC, it is considered 49 iterations to perform correctly, and every iteration has 48 FPOs related to the prediction estimation, the cost function reduction and the second step prediction process. For PCC-VV, it is considered 13 iterations with 121 FPOs and for M2PC and N-M2PC, it is considered 12 iterations with 164 and 228 FPOs respectively.

TABLE X
COMPARATIVE ANALYSIS OF AVERAGE SWITCHING FREQUENCY (KHZ) OF CLASSIC PCC, PCC-VV, M2PC AND N-M2PC AT DIFFERENT SPEEDS (RPM) AND SAMPLING FREQUENCIES (KHZ).

ω_m^*	PCC	PCC-VV	M2PC	N-M2PC
Sampling frequency of 8 kHz				
500	2.8	3.7	8	1.35
1000	2.7	3.5	8	1.32
1500	–	3.2	8	1.3
2000	–	–	–	1.28
Sampling frequency of 16 kHz				
500	5.3	6.9	16	2.63
1000	5.15	6.5	16	2.6
1500	4.75	6.2	16	2.5
2000	–	5.8	16	2.37

At last, Table X shows a comparative analysis of the average switching frequency for classic PCC, PCC-VV, M2PC and N-M2PC at different rotor speeds, where the results show a lower switching frequency for lower sampling frequency and higher speeds, due to the fact that the larger voltage vectors are more used in those operation points. As presented in [34], M2PC is a fixed switching frequency technique which maintains the amount of the sampling frequency, due to the fact that it uses null vector, generating less harmonic content, but limiting the sampling range according to the transistor type. As for N-M2PC, the switching frequency is lower, due to the fact it only uses the large and mid vectors, diminishing the semiconductor stress and losses.

VII. CONCLUSION

This paper proposed a novel modulated MPC technique applied to an ASIMD. This technique has been designed to improve the steady-state error in the $(d-q)$ stator currents and effectively reducing the $(x-y)$ sub-space using VL and VM of the $(\alpha-\beta)$ sub-space. The experimental results showed the performance of the proposed technique compared to another modulated technique presented as M2PC, PCC-VV and to classic PCC, where the tests have been done under different operation points (steady and transient conditions) including low and high mechanical speeds, sampling frequencies and tuning parameters for $(x-y)$ stator currents, respectively. As shown in the results, M2PC and PCC-VV are excellent alternatives to classic PCC for low mechanical speeds, specially M2PC which performs excellent in the $(\alpha-\beta)$ sub-space, where all the figures of merit prove a better performance than classic PCC and N-M2PC. However, there is a limitation in terms of high mechanical speeds and higher sampling frequencies, where M2PC worsens its performance, due to the fact that it fixes the switching frequency from the sampling frequency, aggravating the switching losses. On the other hand, N-M2PC is proven to be a great alternative to classic PCC, PCC-VV and M2PC in high mechanical speeds, specially at higher sampling frequencies, where the performance in terms of steady-state error and $(x-y)$ currents minimization are good proving that at lower sampling frequency, it can still perform with stability, unlike classic PCC

and M2PC. In transient condition, the results demonstrated a good transient current behavior in terms of response time, where classic PCC is the fastest, followed by N-M2PC. In summary, M2PC presents an excellent performance to be a good alternative in low mechanical speeds up to 1500 rpm (25 Hz, 1 pole pair) and N-M2PC is proven to be a great alternative for high speeds, above 1500 rpm, for industrial applications.

Acknowledgment

The authors would like to thank the Consejo Nacional de Ciencia y Tecnología (CONACYT)-Paraguay, Grant Number POSG16-05 and FONDECYT Regular 1160690 Research Project.

References

[1] E. Levi, "Advances in converter control and innovative exploitation of additional degrees of freedom for multiphase machines," *IEEE Trans. Ind. Electron.*, vol. 63, DOI 10.1109/TIE.2015.2434999, no. 1, pp. 433–448, 2016.

[2] I. Subotic, N. Bodo, E. Levi, B. Dumnic, D. Milicevic, and V. Katic, "Overview of fast on-board integrated battery chargers for electric vehicles based on multiphase machines and power electronics," *Elect. Power Appl.*, vol. 10, DOI 10.1049/iet-epa.2015.0292, no. 3, pp. 217–229, 2016.

[3] E. Levi, R. Bojoi, F. Profumo, H. Toliyat, and S. Williamson, "Multiphase induction motor drives–a technology status review," *Elect. Power Appl.*, vol. 1, DOI 10.1049/iet-epa:20060342, no. 4, pp. 489–516, 2007.

[4] A. G. Yepes, A. Vidal, J. Malvar, O. López, and J. Doval-Gandoy, "Tuning method aimed at optimized settling time and overshoot for synchronous proportional-integral current control in electric machines," *IEEE Trans. Power Electron.*, vol. 29, DOI 10.1109/TPEL.2013.2276059, no. 6, pp. 3041–3054, 2014.

[5] F. Barrero, J. Prieto, E. Levi, R. Gregor, S. Toral, M. J. Durán, and M. Jones, "An enhanced predictive current control method for asymmetrical six-phase motor drives," *IEEE Trans. Ind. Electron.*, vol. 58, DOI 10.1109/TIE.2010.2089943, no. 8, pp. 3242–3252, 2010.

[6] F. Barrero, M. R. Arahal, R. Gregor, S. Toral, and M. J. Durán, "A proof of concept study of predictive current control for VSI-driven asymmetrical dual three-phase AC machines," *IEEE Trans. Ind. Electron.*, vol. 56, DOI 10.1109/TIE.2008.2011604, no. 6, pp. 1937–1954, 2009.

[7] C. S. Lim, E. Levi, M. Jones, N. A. Rahim, and W. P. Hew, "FCS-MPC-based current control of a five-phase induction motor and its comparison with PI-PWM control," *IEEE Trans. Ind. Electron.*, vol. 61, DOI 10.1109/TIE.2013.2248334, no. 1, pp. 149–163, 2013.

[8] E. Fuentes, C. A. Silva, and R. M. Kennel, "MPC implementation of a quasi-time-optimal speed control for a PMSM drive, with inner modulated-fs-mpc torque control," *IEEE Trans. Ind. Electron.*, vol. 63, DOI 10.1109/TIE.2016.2519326, no. 6, pp. 3897–3905, 2016.

[9] J. Rodas, F. Barrero, M. R. Arahal, C. Martín, and R. Gregor, "Online estimation of rotor variables in predictive current controllers: a case study using five-phase induction machines," *IEEE Trans. Ind. Electron.*, vol. 63, DOI 10.1109/TIE.2016.2559420, no. 9, pp. 5348–5356, 2016.

[10] I. Gonzalez-Prieto, M. J. Duran, J. J. Aciego, C. Martin, and F. Barrero, "Model predictive control of six-phase induction motor drives using virtual voltage vectors," *IEEE Trans. Ind. Electron.*, vol. 65, DOI 10.1109/TIE.2017.2714126, no. 1, pp. 27–37, 2018.

[11] I. Gonzalez-Prieto, M. J. Duran, J. J. Aciego, C. Martin, and F. Barrero, "Model predictive control of six-phase induction motor drives using virtual voltage vectors," *IEEE Trans. Ind. Electron.*, vol. 65, DOI 10.1109/TIE.2017.2714126, no. 1, pp. 27–37, 2017.

[12] J. J. Aciego, I. G. Prieto, and M. J. Duran, "Model predictive control of six-phase induction motor drives using two virtual voltage vectors," *IEEE Journal of Emerging and Selected Topics in Power Electronics*, vol. 7, DOI 10.1109/JESTPE.2018.2883359, no. 1, pp. 321–330, 2018.

[13] I. González-Prieto, M. Durán, M. Bermúdez, F. Barrero, and C. Martín, "Assessment of Virtual-Voltage-based Model Predictive Controllers in Six-phase Drives under Open-Phase Faults," *IEEE Journal of Emerging and Selected Topics in Power Electronics*, DOI 10.1109/JESTPE.2019.2915666, 2019.

[14] S. Toledo, M. Rivera, J. Muñoz, R. Peña, J. Riveros, and R. Gregor, "Fixed switching frequency predictive control for a multi-drive indirect matrix converter system," in *Proc. SPEC*, DOI 10.1109/SPEC.2017.8333672, 2017, pp. 1–6.

[15] M. Ayala, J. Rodas, R. Gregor, J. Doval-Gandoy, O. Gonzalez, M. Saad, and M. Rivera, "Comparative study of predictive control strategies at fixed switching frequency for an asymmetrical six-phase induction motor drive," in *Proc. IEMDC*, DOI 10.1109/IEMDC.2017.8002121, 2017, pp. 1–8.

[16] F. Gavilan, D. Caballero, S. Toledo, E. Maqueda, R. Gregor, J. Rodas, M. Rivera, and I. Araujo-Vargas, "Predictive power control strategy for a grid-connected 2l-vsi with fixed switching frequency," in *Proc. ROPEC*, DOI 10.1109/ROPEC.2016.7830631, 2016, pp. 1–6.

[17] L. Comparatore, R. Gregor, J. Rodas, J. Pacher, A. Renault, and M. Rivera, "Model based predictive current control for a three-phase cascade H-bridge multilevel statcom operating at fixed switching frequency," in *Proc. PEDG*, DOI 10.1109/PEDG.2017.7972540, 2017, pp. 1–6.

[18] M. Rivera, S. Toledo, C. Baier, L. Tarisciotti, P. Wheeler, and S. Verne, "Indirect predictive control techniques for a matrix converter operating at fixed switching frequency," in *Proc. PRECEDE*, DOI 10.1109/PRECEDE.2017.8071101, 2017, pp. 13–18.

[19] O. Gonzalez, M. Ayala, J. Rodas, R. Gregor, G. Rivas, and J. Doval-Gandoy, "Variable-speed control of a six-phase induction machine using predictive-fixed switching frequency current control techniques," in *Proc. PEDG*, DOI 10.1109/PEDG.2018.8447837, 2018, pp. 1–6.

[20] J. Rodriguez, M. P. Kazmierkowski, J. R. Espinoza, P. Zanchetta, H. Abu-Rub, H. A. Young, and C. A. Rojas, "State of the art of finite control set model predictive control in power electronics," *IEEE Trans. Ind. Inform.*, vol. 9, DOI 10.1109/TII.2012.2221469, no. 2, pp. 1003–1016, 2013.

[21] S. Vazquez, J. Rodriguez, M. Rivera, L. G. Franquelo, and M. Norambuena, "Model predictive control for power converters and drives: Advances and trends," *IEEE Trans. Ind. Electron.*, vol. 64, DOI 10.1109/TIE.2016.2625238, no. 2, pp. 935–947, 2017.

[22] Y. Zhao and T. Lipo, "Space vector PWM control of dual three-phase induction machine using vector space decomposition," *IEEE Trans. Ind. Electron.*, vol. 31, DOI 10.1109/28.464525, no. 5, pp. 1100–1109, 1995.

[23] C. Martín, M. R. Arahal, F. Barrero, and M. J. Durán, "Multiphase rotor current observers for current predictive control: A five-phase case study," *Control Eng. Prac.*, vol. 49, DOI 10.1016/j.conengprac.2016.01.011, pp. 101–111, 2016.

[24] J. Rodas, C. Martin, M. R. Arahal, F. Barrero, and R. Gregor, "Influence of covariance-based ALS methods in the performance of predictive controllers with rotor current estimation," *IEEE Trans. Ind. Electron.*, vol. 64, DOI 10.1109/TIE.2016.2636205, no. 4, pp. 2602–2607, 2017.

[25] J. Rodriguez and P. Cortes, *Predictive control of power converters and electrical drives*. John Wiley & Sons, 2012, DOI 10.1002/9781119941446, vol. 40.

[26] M. Novak, T. Dragicevic, and F. Blaabjerg, "Weighting factor design based on Artificial Neural Network for Finite Set MPC operated 3L-NPC converter," in *Proc. APEC)*, DOI 10.1109/APEC.2019.8722062. IEEE, 2019, pp. 77–82.

[27] B. Majmunović, T. Dragičević, and F. Blaabjerg, "Multi Objective Modulated Model Predictive Control of Stand-Alone Voltage Source Converters," *IEEE Journal of Emerging and Selected Topics in Power Electronics*, DOI 10.1109/JESTPE.2019.2925603, 2019.

[28] C. Martin, M. Arahal, F. Barrero, and M. Duran, "Five-phase induction motor rotor current observer for finite control set model predictive control of stator current," *IEEE Trans. Ind. Electron.*, vol. 63, DOI 10.1109/TIE.2016.2536578, no. 7, pp. 4527–4538, 2016.

[29] A. G. Yepes, J. A. Riveros, J. Doval-Gandoy, F. Barrero, O. López, B. Bogado, M. Jones, and E. Levi, "Parameter identification of multiphase induction machines with distributed windings Part 1: Sinusoidal excitation methods," *IEEE Trans. Energy Conv.*, vol. 27, DOI 10.1109/TEC.2012.2220967, no. 4, pp. 1056–1066, 2012.

[30] J. A. Riveros, A. G. Yepes, F. Barrero, J. Doval-Gandoy, B. Bogado, O. Lopez, M. Jones, and E. Levi, "Parameter identification of multiphase induction machines with distributed windings Part 2: Time-domain techniques," *IEEE Trans. Energy Conv.*, vol. 27, DOI 10.1109/TEC.2012.2219862, no. 4, pp. 1067–1077, 2012.

[31] M. Ayala, J. Doval-Gandoy, J. Rodas, O. Gonzalez, and R. Gregor, "Current control designed with model based predictive control for six-phase motor drives," *ISA transactions*, DOI 10.1016/j.isatra.2019.08.052, 2019.

[32] B. Bogado, F. Barrero, M. Arahal, S. Toral, and E. Levi, "Sensitivity to electrical parameter variations of predictive current control in multiphase drives," in *Proc. IECON*, DOI 10.1109/IECON.2013.6699982. IEEE, 2013, pp. 5215–5220.
[33] F. Wang, Z. Zhang, X. Mei, J. Rodríguez, and R. Kennel, "Advanced control strategies of induction machine: Field oriented control, direct torque control and model predictive control," *Energies*, vol. 11, DOI 10.3390/en11010120, no. 1, p. 120, 2018.
[34] O. Gonzalez, M. Ayala, J. Doval-Gandoy, J. Rodas, R. Gregor, and M. Rivera, "Predictive-Fixed Switching Current Control Strategy Applied to Six-Phase Induction Machine," *Energies*, vol. 12, DOI 10.3390/en12122294, no. 12, p. 2294, 2019.

Magno Ayala received the B.Eng. degree in electronic engineering from the Universidad Nacional de Asunción (UNA), Paraguay, in 2014 and his M.Sc. in 2017. He joined the Laboratory of Power and Control System at the UNA, in 2015, working as a Research Assistant. Mr. Ayala is a recipient of the training program for university lecturers from the CONACYT of Paraguay for his Ph.D. studies.

Jesús Doval-Gandoy (M'99) received the M.Sc. degree from Polytechnic University of Madrid, Madrid, Spain, in 1991 and the Ph.D. degree from the University of Vigo, Vigo, Spain in 1999.

From 1991 till 1994 he worked at industry. He is currently the head of the Applied Power Electronics Technology Research Group, University of Vigo. His research interests are in the areas of ac power conversion.

Jorge Rodas (S'08–M'12–SM'19) was born in Asunción, Paraguay in 1984. He received his B.Eng. degree in Electronic Engineering from the Universidad Nacional de Asunción (UNA), Paraguay, in 2009. He received his M.Sc. degrees from the Universidad de Vigo, Spain, in 2012 and from the Universidad de Sevilla, Spain, in 2013, and his joint-university Ph.D. degree between the Universidad Nacional de Asunción and the Universidad de Sevilla in 2016.

In 2011, he joined the Laboratory of Power and Control Systems, Faculty of Engineering, UNA, where he currently serves as a Full Professor.

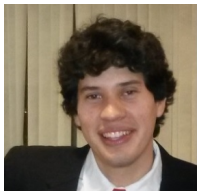

Osvaldo Gonzalez was born in Paraguay in 1987. B.Eng. degree in electronic engineering from the Universidad Nacional de Asunción (UNA), in 2014 and the M.Sc. degree in Power Electronics in 2017. His research interests include the area of control of multiphase motors. Mr. Gonzalez is a recipient of the training program for university lecturers from the CONACYT of Paraguay for his Ph.D. studies.

Raúl Gregor was born in Asunción, Paraguay, in 1979. He received the Bachelor Degree in Electronic Engineering from the Catholic University of Asunción, Paraguay, in 2005. He received the M.Sc. and Ph.D. degrees in Electronic, Signal Processing and Communications from the Higher Technical School of Engineering (ETSI), University of Seville, Spain, in 2008 and 2010, respectively. Since March 2010, Prof. Gregor is Head of the Laboratory of Power and Control System (LSPyC) of the Engineering Faculty in the National University of Asunción, Paraguay.

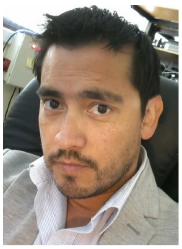

Marco Rivera was born in Talca, Chile, in 1982. He received the B.Sc. degree in electronics engineering and the M.Sc. degree in electrical engineering from the Universidad de Concepción, Concepción, Chile, in 2007 and 2008, respectively, and the Ph.D. degree from the Department of Electronics Engineering, Universidad Técnica Federico Santa María, Valparaíso, Chile, in 2011.